An examination of alternative schemes for active and semi-active control of vertical car-body vibration to improve ride comfort

Bin Fu, Stefano Bruni,
Dipartimento di Meccanica, Politecnico di Milano, Via La Masa 1, Milano, 20156, Italy
bin.fu@polimi.it

Version accepted for publication on:
Proceedings of the Institution of Mechanical Engineers, Part F: Journal of Rail and Rapid Transit
Volume: 236 issue: 4, page(s): 386-405
https://doi.org/10.1177/09544097211022108

Abstract: The recent tendency to reduce the weight of car bodies is posing a new challenge to vertical ride quality, since the vibrations related to car-body vertical bending modes affect heavily passengers' comfort and cannot be fully mitigated by conventional vehicle suspensions. In this work, four mechatronic suspensions, considering active and semi-active technologies in secondary and primary suspensions, are compared to show their relative merits. *LQG* and $H\infty$ model-based control strategies are established in a consistent way for each suspension scheme to perform a comparative assessment of the four concepts on objective grounds. A two-dimensional 9-DOF vehicle model is firstly built, using a simplified representation of car-body bending modes; this model is also used to design the model-based controllers. The comparison of the four mechatronic suspension schemes based on the 9-DOF model shows that full-active secondary suspensions is the most effective solution whilst semi-active primary suspensions are also effective in terms of mitigating car-body bending vibration. Then, a three-dimensional flexible multibody systems (FMBS) vehicle model integrated with a finite-element car-body is considered to allow a more detailed consideration of the vehicle's vibrating behaviour. The results of the FMBS model show a good agreement to the results of the 9-DOF model and the relative merits of the four mechatronic

suspension schemes as found from the previous analysis are basically confirmed, although the FMBS model is more suited for a quantitative assessment of ride quality.

Keywords*: active suspension; semi-active primary suspension; ride comfort; flexible car-body; LQG control; H∞ control*

1 Introduction

Active and semi-active control technologies can be used to improve the performance of railway vehicles under different respects including stability, curving behaviour and ride quality[1,2]. As far as the improvement of ride quality is concerned, active lateral suspensions have been successfully implemented in Japan and Europe, while in some other countries full-scale tests have been carried in the line or on roller rigs [3]. By contrast, active vertical suspension received so far relatively less attention, and this is possibly due to the fact that pneumatic secondary suspensions in use in most modern-generation passenger trains are capable of providing an adequate level of ride quality in most service scenarios. However, the recent tendency to reduce the weight of car bodies is posing a new challenge to ensuring proper ride quality levels, as the lighter car bodies are more prone to vibrations involving their vertical bending modes in a frequency range relevant to ride quality [4,5], which can hardly be controlled by passive suspensions whilst mechatronic suspensions can be effective with controlling the narrow band of excitation related to selected car-body modes [6].

Previous research concerned with active and semi-active vertical suspensions for railway vehicles is summarized hereinafter. Goodall built a simplified rigid vehicle model and compared the effectiveness of the full active and semi-active control for vertical secondary suspension, showing that, active and semi-active suspension can respectively achieve 50% and 34% improvement, in terms of reduction of RMS acceleration[7]. In Sweden, the active vertical secondary suspension was tested on Regina 250 with the speed up to 200 km/h, where the passive vertical dampers between car-bodies and bogies are replaced by actuators [8]. Skyhook control is integrated with mode separation so that car-body bounce, pitch and roll motions are controlled

separately. The vibrations coming from both car-body rigid vibrations and structural vibrations are improved.

The above-mentioned investigations focus on car-body rigid vibrations. However, in case the objective is to reduce vibration caused by car-body flexibility, the control strategies are quite different. One method is to implement piezoelectric actuators [9,10], in which strain sensors measure structural vibration and then the bending moment required to attenuate car-body vibration is generated by piezoelectric actuators. Foo and Goodall explored the use of a classic active secondary suspension with Skyhook controller, showing a limited reduction of car-body structural vibration. The same authors introduced an actively-controlled mass-damper structure attached to the car-body which proves more effective to suppress the bending mode [11]. References [12,13] adopt the same approach through a properly designed passive or semi-active suspension for the electrical converter attached to the car-body underfloor. Sugahara proposed to use semi-active primary suspension to improve the car-body bending modes [6,14,15] for a high-speed train running on Shinkansen line at speeds up to 300 km/h, as well as for a meter-gauged vehicle with the maximum speed at 100km/h. Although primary suspension is rarely considered for improving ride quality, the simulations and filed tests by Sugahara demonstrate the effectiveness of this scheme.

The state-of-art analysis above shows that many different approaches can be successful in controlling the vertical vibration of the car-body in relation to its rigid and flexible modes. Full-active and semi-active suspensions can both be used, and mechatronic components can be included both in the primary and secondary suspensions. Therefore, four main schemes can be devised: active primary, semi-active primary, active secondary and semi-active secondary suspensions. Although there may be practical reasons for choosing one or another of these schemes, it is important to investigate the relative merits of each one of these solutions.

The aim of this paper is therefore to perform an objective comparison of the benefits of each one of the above schemes that can be hopefully used as a basis to drive the design of future

mechatronic suspension concepts and to identify new solutions not addressed by previous research work. To this aim, the case of a trailer vehicle designed for a maximum speed of 120 km/h is analysed. The control strategies considered in this study are LQG and H∞, as they both allow to define the objectives of the mechatronic suspension in a way that enables an objective comparison of the active and semi-active suspension schemes. Based on the use of these two control strategies, the same control target is defined for all suspension schemes, i.e. to minimize a weighted sum of the car-body acceleration measured at front, centre and rear positions and of the control force. In this way, the performance of the four suspension schemes can be directly compared.

Initial analyses are performed using a simplified vehicle model with 9 degrees of freedom (DOF) and a systematic comparison of the different suspension schemes is worked out thanks to the low computational effort required by this model. Both LQG and H∞ are applied on the simplified model to show the improvement of ride comfort that can be achieved using different suspension schemes for an ideal case in which the design of the controller involves no modelling error or uncertainty. Then, a more detailed flexible multi-body system (FMBS) model of the same vehicle is used to consider in more depth the effect of car-body flexibility, as well as the influence of some specific features of the vehicle's suspensions that cannot be represented to the desired level of accuracy by the simplified model. For the FMBS analysis, the H∞ controller is adopted to evaluate the performance of candidate suspension schemes, in view of analysing the applicability of the schemes in a real application.

2 Rail vehicle dynamic models

2.1 Simplified 9-DOF vehicle model

In this study, a simplified 9-DOF vehicle model is firstly considered, see Figure 1. This model considers the bounce and pitch motion of the car-body(coordinates Z_c, θ_c), the same motion components for the two bogies (coordinates $Z_{t1}, \theta_{t1}, Z_{t2}, \theta_{t2}$), and the first three flexible car-body

bending modes (coordinates q_1, q_2, q_3). The vertical displacements of the four wheelsets ($Z_{w1}, Z_{w2}, Z_{w3}, Z_{w4}$) are assumed to follow the shape of the longitudinal level track irregularity. When full-active or semi-active suspensions are considered, some of the passive dampers shown in Figure 1 are replaced by actuators or adjustable dampers.

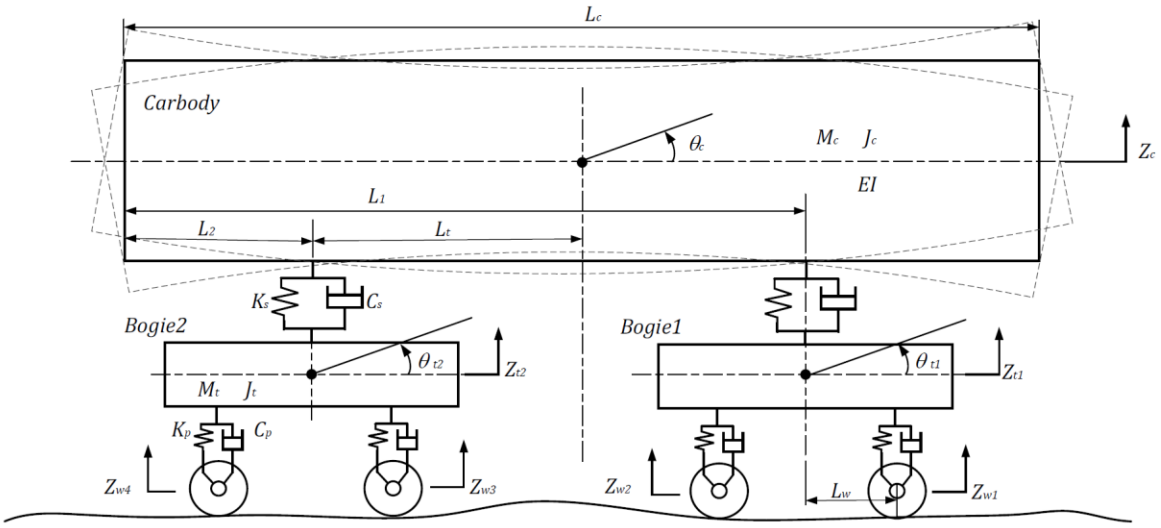

Figure 1: The 9-DOF of vehicle model

The values of the physical parameters of the 9-DOF model are listed in Table 1 using the nomenclature introduced in Figure 1. These parameters are chosen to produce a simplified representation of the FMBS vehicle model introduced in Section 2.2.

Table 1 Parameters of 9-DOF model

Symbol	Explanation	Value
M_c	Mass of car-body	34.25 [t]
J_c	Inertia of car-body	2.3×10^6 [kg$\cdot m^2$]
M_t	Mass of bogie	3 [t]
J_t	Inertia of bogie	2200 [kg$\cdot m^2$]
C_s	Damping of secondary suspension	80 [kNs/m]
C_p	Damping of primary suspension	30 [kNs/m]
K_s	Stiffness of secondary suspension	0.7 [MN/m]
K_p	Stiffness of primary suspension	2.6 [MN/m]
EI	Car-body bending moment	3.4×10^9 [N$\cdot m^2$]
μI	Car-body viscous damping coefficient	2.4×10^6 [N$\cdot m^2 \cdot s/rad$]
L_c	Car-body length	25 [m]
L_t	Half distance between two bogie centre	9.5[m]

L_w	Half distance of wheelbase	1.25[m]
L_1	Distance from car-body rear end to front bogie	22[m]
L_2	Distance from car-body rear end to rear bogie centre	3[m]

The first three car-body bending modes are defined considering the car-body as Euler beam with Free-Free boundary conditions. Using the modal superposition, the following expression is obtained for the car-body vertical displacement $W(x,t)$ at position x time t due to the bending flexibility [16]:

$$W(x,t) = \sum_{i=1,3} Y_i(x) q_i(t) \tag{1}$$

where $Y_i(x)$ is the shape of the i^{th} bending mode, defined according to Eq. (2):

$$Y_i(x) = (\cos\beta_i x + \cosh\beta_i x) - \frac{\cos\beta_i L_c - \cosh\beta_i L_c}{\sin\beta_i L_c - \sinh\beta_i L_c}(\sin\beta_i x + \sinh\beta_i x) \tag{2}$$

with $\beta_1 L_c = 4.7300;\ \beta_2 L_c = 7.8532;\ \beta_3 L_c = 10.9956.$

According to Eq. (2), the shapes of the first three car-body bending modes are illustrated in Figure 2.

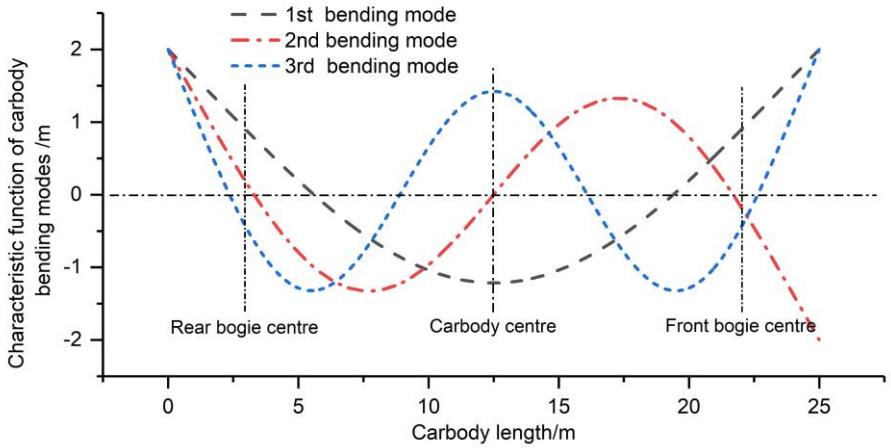

Figure 2 Modal shapes of the first three car-body bending modes

The equations governing the variation in time of the coordinates $q_i(t)$ describing the flexible vibration is shown in Eq. (3)

$$\ddot{q}_i + 2\xi_i\omega_i\dot{q}_i + {\omega_i}^2 q_i = \frac{F_{s1}Y_i(L_1)}{M_c} + \frac{F_{s2}Y_i(L_2)}{M_c} \tag{3}$$

where F_{s1} and F_{s2} refer to the forces of secondary suspension; ω_i and ξ_i are the natural frequencies and damping ratio of the three bending modes, which are derived according to Eq. (4). In Figure 2, we can see that the bending curves do not cross the neutral layer at the positions L_1 and L_2, which means that $Y_i(L_1)$ and $Y_i(L_2)$ in Eq.(3) are nonzero values and the three bending modes are controllable in principle.

$$\begin{cases} \omega_i = \beta_i^{\,2}\sqrt{\frac{EIL_c}{M_c}} \\ \xi_i = \frac{\mu I}{2EI}\omega_i \end{cases} \tag{4}$$

According to the above equations, natural frequencies for three bending modes are derived at 9.0Hz, 24.7Hz and 48.5Hz. It should be noted that as far as ride comfort is concerned, the 2nd and 3rd bending modes are far less important than the first bending mode since harmonic components of car body vibration falling in the frequency range above 20Hz have a minor influence on ride comfort [4,17]. Nevertheless, the 2nd and 3rd bending modes are also considered in the simplified model, to consider the effect of high-frequency vibration of the car body which might have an impact on the performance of the active or semi-active suspensions.

The equations governing the variation in time of the 6 coordinates describing the rigid motion of the car-body and bogies are:

$$\begin{cases} M_c\ddot{Z}_c = F_{s1} + F_{s2} & (Carbody\ bounce) \\ J_c\ddot{\theta}_c = L_tF_{s1} - L_tF_{s2} & (Carbody\ pitch) \\ M_t\ddot{Z}_{t1} = -F_{s1} + F_{p1} + F_{p2} & (Bogie1\ bounce) \\ J_t\ddot{\theta}_{t1} = L_wF_{p1} - L_wF_{p2} & (Bogie1\ pitch) \\ M_t\ddot{Z}_{t2} = -F_{s2} + F_{p3} + F_{p4} & (Bogie2\ bounce) \\ J_t\ddot{\theta}_{t2} = L_wF_{p3} - L_wF_{p4} & (Bogie2\ pitch) \end{cases} \tag{5}$$

where F_{p1} to F_{p4} express the forces of primary suspension.

The car-body acceleration is derived from the superposition of car-body rigid modes and bending modes. Particularly important in view of the definition of the regulators, are the acceleration of the car-body over the front and rear bogies and at car-body centre, $\ddot{Z}_{cf}(t)$, $\ddot{Z}_{cr}(t)$ and $\ddot{Z}_{cc}(t)$ respectively:

$$\begin{cases} \ddot{Z}_{cf}(t) = \ddot{Z}_c(t) + L_t\ddot{\theta}_c + \sum_{i=1}^{3} Y_i(L_1)\,\ddot{q}_i(\mathrm{t}) \\ \ddot{Z}_{cr}(t) = \ddot{Z}_c(t) - L_t\ddot{\theta}_c + \sum_{i=1}^{3} Y_i(L_2)\,\ddot{q}_i(\mathrm{t}) \\ \ddot{Z}_{cc}(t) = \ddot{Z}_c(t) + \sum_{i=1}^{3} Y_i(L_1/2 + L_2/2)\,\ddot{q}_i(\mathrm{t}) \end{cases} \tag{6}$$

The forces from the secondary suspension and primary suspension are computed according to Eq. (7), in which u_{s1} and u_{s2} are input control forces for active or semi-active secondary suspension and u_{p1} to u_{p4} are control forces for active or semi-active primary suspension.

$$\begin{cases} F_{s1} = C_s[\dot{Z}_{t1} - (\dot{Z}_c + L_t\dot{\theta}_c + \sum_{i=1}^{3} Y_i(L_1)\dot{q}_i)] + K_s[Z_{t1} - (Z_c + L_t\theta_c + \sum_{i=1}^{3} Y_i(L_1)\,q_i)] + u_{s1} \\ F_{s2} = C_s[\dot{Z}_{t2} - (\dot{Z}_c - L_t\dot{\theta}_c + \sum_{i=1}^{3} Y_i(L_2)\dot{q}_i)] + K_s[Z_{t2} - (Z_c - L_t\theta_c + \sum_{i=1}^{3} Y_i(L_2)\,q_i)] + u_{s2} \\ F_{p1} = C_p[\dot{Z}_{w1} - (\dot{Z}_{t1} + L_w\dot{\theta}_{t1})] + K_p[Z_{w1} - (Z_{t1} + L_w\theta_{t1})] + u_{p1} \\ F_{p2} = C_p[\dot{Z}_{w2} - (\dot{Z}_{t1} - L_w\dot{\theta}_{t1})] + K_p[Z_{w2} - (Z_{t1} - L_w\theta_{t1})] + u_{p2} \\ F_{p3} = C_p[\dot{Z}_{w3} - (\dot{Z}_{t2} + L_w\dot{\theta}_{t2})] + K_p[Z_{w3} - (Z_{t2} + L_w\theta_{t2})] + u_{p3} \\ F_{p4} = C_p[\dot{Z}_{w4} - (\dot{Z}_{t2} - L_w\dot{\theta}_{t2})] + K_p[Z_{w4} - (Z_{t2} - L_w\theta_{t2})] + u_{p4} \end{cases} \tag{7}$$

For the control forces u, two simplified models are introduced to reflect the response time of actuators and semi-active damper. For full-active suspension components, a simplified model of actuator dynamics is introduced in the form of a first-order system representing the delay of the actual control action u_a with respect to its reference u_{ref}:

$$\dot{u}_a = -\frac{u_a}{T_r} + \frac{u_{ref}}{T_r} \tag{8}$$

where T_r refers to the response time of actuators.

When the semi-active suspension is implemented, the reference force u_{ref} needs to be transformed into the damping force u_d which is produced by an adjustable damper, capable of adjusting its viscous damping coefficient in a range from a minimum value d_{min} to a maximum value d_{max}. The selection of the desired damping coefficient requires the measure of the piston velocity of the damper v_P, i.e. the relative velocity between the two ends of the damper. This measure can be obtained from a velocity sensor integrated with the damper or from the integration of acceleration signals measured at the end mounts of the damper. In the simplified model, the bogie pitch and bounce motions are obtained to calculate the velocities at the end of damper mounted to the bogies.

$$u_d = \begin{cases} d_{min} v_P & (u_a \cdot v_P < 0) \\ sign(v_P) \cdot \max\left[\min\left(|d_{max} v_P|, |u_{ref}|\right), |d_{min} v_P|\right] & (u_a \cdot v_P \geq 0) \end{cases} \quad (9)$$

In Eq. (9) the minimum and maximum damping values d_{min} and d_{max} are set to 5 kNs/m and 100kNs/m respectively. These values are reasonable and correspond to the damping coefficient of existing products [18,19]. The u_d also need to be processed using a first-order filter in the form of Eq. (8), to consider the effect of delays in the semi-active damper.

2.2 Flexible multibody systems model

In addition to the simplified model, an FMBS model of the same vehicle is built in SIMPACK to provide a more detailed description of vehicle dynamics, see Figure 3. The model considers one car-body, two bogies and four wheelsets, with each body having six degrees of freedom, and eight axle-boxes, rotating with respect to the wheelset axis. A finite element car-body model is integrated to reflect the real car-body flexible modes, considering the first 28 flexible vibration modes of the car-body, which allows reproducing car-body dynamics in the frequency range up to 30 Hz. Besides extending the simplified two-dimensional(2-D) model to three-dimensional (3-D) model, the FMBS model takes into account some detailed arrangement for primary suspension that cannot be reproduced in the simplified model. In vertical direction, a coil spring on the top of the axle-box bears the vertical load. At the outer side of the axle-box, a vertical damper is mounted, and at the inner side of the axle-box a traction rod connects the bogie side beam and the axle-box, providing the primary yaw stiffness. In the secondary suspension, each bogie has two vertical dampers, one lateral damper and one anti-roll bar. The traction link is also considered to transfer the longitudinal force between the bogies and the car-body. Hertz contact and FASTSIM are used to calculate normal and tangent force at wheel-rail interface. Measured track irregularities from a real track with low maintenance quality are considered, including longitudinal level, lateral alignment, cross level and gauge variation. The parameters of the FMBS model are summarized in Appendix 1.

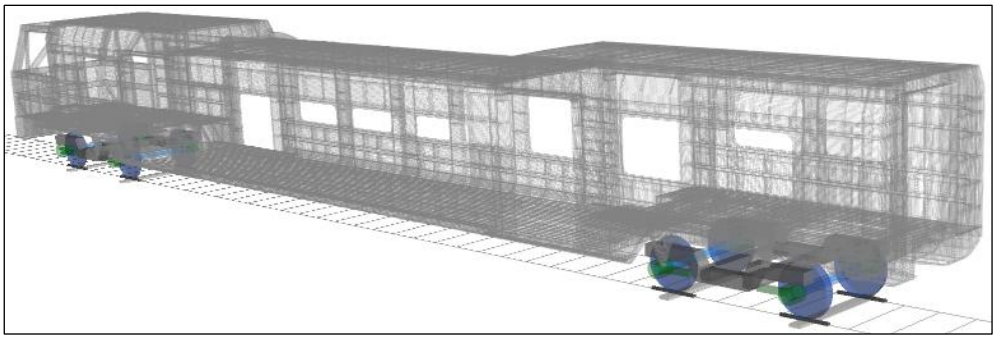

Figure 3 Full scaled vehicle model

2.3 Analysis of passive vehicle models

2.3.1 PSD of car-body acceleration from simplified model

The vertical acceleration of the car-body at front, centre and rear position are evaluated according to Eq. (6) and the corresponding. power spectral density (PSD) curves are shown in Figure 4. The PSD curves are processed using Periodogram method using a Hanning window with a setting of 5-second window length and 0.5 overlap rate.

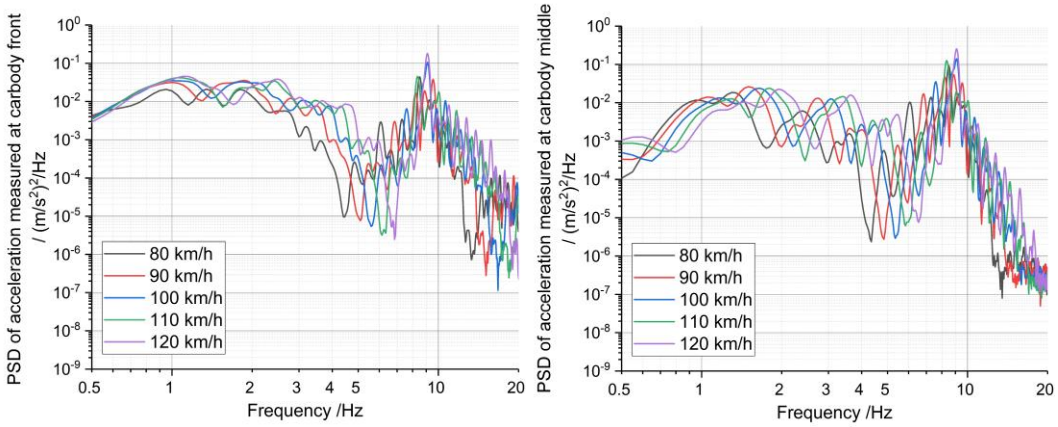

(a) *(b)*

Figure 4 PSDs of vertical car-body acceleration from the 9-DOF model: (a) Car-body front (b) Car-body centre

As shown in Figure 4, the low-frequency car-body rigid vibrations and car-body first bending mode at 9Hz are mostly excited by track irregularities, and the maximum peak value of the PSD at 9 Hz is affected by vehicle speed and takes a maximum value for vehicle speed 120km/h. The car-body pitch motion resonates at approximately 0.9Hz and affects mainly the acceleration at car-body front (above bogie centre), whereas the first bending mode causes more intensive vibration at car-

body centre, consistently with its modal shape shown in Figure 2. The vehicle vibration at speed of 120km/h is used as the reference for further analyses.

2.3.2 Comparison between simplified model and full-scaled vehicle model

In this section, the results obtained from the 9-DOF and the FMBS models of the vehicle in passive configuration are compared in terms of the PSDs of car-body acceleration at 120km/h, see Figure 5. On one hand, the differences show the influence of dynamic effects not considered in the simplified model: the FMBS model includes a larger number of flexible modes for the car-body, resulting in more intense dynamics above 15Hz compared to the simplified model. However, in the frequency range below 15Hz, a quite good agreement between the two models is observed, justifying the use of the simplified model for the design of model-based controllers (see Section 3) and also to perform an initial exploratory analysis of the benefits of semi-active and active suspension control.

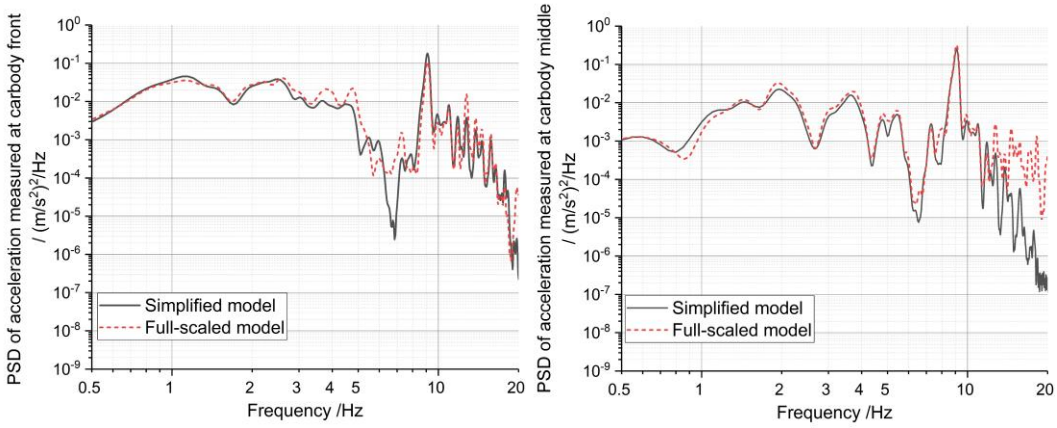

(a) *(b)*

Figure 5 Comparison of PSDs of vertical acceleration at 120km/h for the 9-DOF and FMBS models at (a) car-body front and (b) car-body centre positions

3 Control strategies for active suspensions

Two model-based control strategies, namely LQG and H∞, are considered in this work as they allow a similar implementation for both full-active and semi-active control in secondary and

primary suspensions, allowing an objective comparison of the alternative approaches to improving ride quality.

3.1 LQG control

The Linear Quadratic Gaussian (LQG) controller consists of the integration of the Linear Quadratic Regulator (LQR) and state estimation based on the Kalman filter [20,21]. In LQR, a linear feedback of the system's full state is applied, with the objective of minimising a linear quadratic cost function *J* which involves a measure of the system's performance to be improved and a measure of the control force/effort to be reduced. Assuming the observation of the full state of the system is not feasible or practical, a Kalman filter is used to estimate the system's state variables based on a reduced set of measurements. The schematic diagram of LQG control is shown in Figure 6.

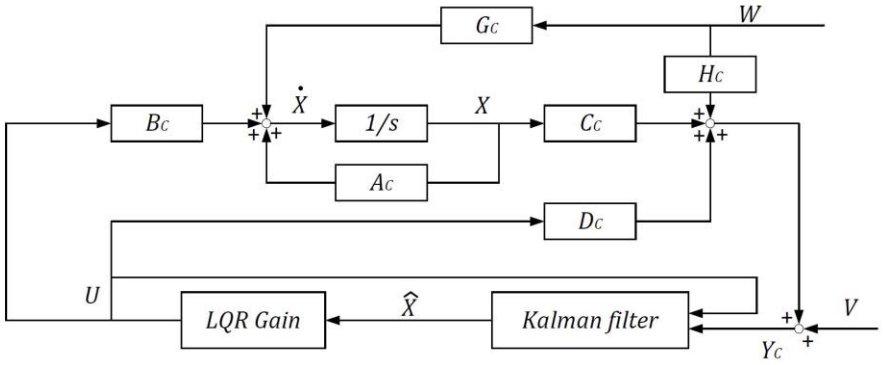

Figure 6 Schematic diagram of LQG control

The state-space equations of the vehicle model are derived in form of Eq. (10) according to the equations of the 9-DOF model introduced in Section 2.1:

$$\dot{X} = A_C X + B_C U + G_C W \tag{10}$$

where X represents the state vector collecting the 18 state variables of the model; U is the vector of control forces from the active or semi-active suspensions; W is the disturbance coming from track irregularities, see Eq. (11) to (13) for the three matrixes.

$$X = [Z_c \quad \dot{Z_c} \quad \theta_c \quad \dot{\theta_c} \quad Z_{t1} \quad \dot{Z_{t1}} \quad \theta_{t1} \quad \dot{\theta_{t1}} \quad Z_{t2} \quad \dot{Z_{t2}} \quad \theta_{t2} \quad \dot{\theta_{t2}} \quad q_1 \quad \dot{q_1} \quad q_2 \quad \dot{q_2} \quad q_3 \quad \dot{q_3}]^T \tag{11}$$

$$U = [u_{s1}, u_{s2}]^T \quad \text{or} \quad U = \left[u_{p1}, u_{p2}, u_{p3}, u_{p4}\right]^T \tag{12}$$

$$W = [\dot{Z_{w1}}, \dot{Z_{w2}}, \dot{Z_{w3}}, \dot{Z_{w4}}, Z_{w1}, Z_{w2}, Z_{w3}, Z_{w4}]^T \tag{13}$$

The cost function of LQR is defined as:

$$J_{LQR} = \lim_{t \to \infty} \frac{1}{t} \int_0^t ({Y_t}^T Q Y_t + U^T R U)\, dt \tag{14}$$

where Y_t is the vector of the indexes used to describe the performance of the system which is in this case represented by the acceleration of the car-body over the two bodies and at in the centre position:

$$Y_t = [\ddot{Z}_{cf}, \ddot{Z}_{cc}, \ddot{Z}_{cr}]^T \tag{15}$$

and Q and R are diagonal matrices defining the relative importance of vectors Y_t and U in the definition of the total cost function J_{LQR}. In this study, an equal weight is chosen in matrix Q for the acceleration of the car-body at the three positions.

A feedback control gain K_{LQR} is calculated to minimize the cost function J_{LQR} by solving the Riccati Equation [21]. Then, the ideal control forces U are obtained by Eq. (16)

$$U = -K_{LQR} \hat{X} \tag{16}$$

where $\hat{X}$ is the estimation of the state vector X obtained from the Kalman filter.

As far as state estimation is concerned, it is observed that in the 9-DOF model the pitch motion of the two bogies are not affecting car-body vibration and therefore the state variables associated with bogie pitch motions have no contribution to the control force. In other words, we don't need to observe the full-state vehicle system but a sub-system with removal of bogie pitch motions.

A 5-sensor measuring set-up is proposed for the Kalman filter, using three accelerometers mounted on the car-body at the same positions considered in the definition of the control target Y_t , and two accelerometers mounted on the centre of the two bogies, $\ddot{Z}_{b1}$ and $\ddot{Z}_{b2}$ respectively. The resulting measurement vector is:

$$Y_c = [\ddot{Z}_{cf}, \ddot{Z}_{cc}, \ddot{Z}_{cr}, \ddot{Z}_{b1}, \ddot{Z}_{b2}]^T = \ C_c X + D_C U + H_C W + V \tag{17}$$

where the vector V represents the measuring noise.

3.2 $H\infty$ Control

Although the LQG controller can provide excellent performance in ideal condition, it might be bothered with robustness issue, in case the stability margins are reduced by the effect of uncertainties in the vehicle model, such as fluctuations of the car-body mass or deviation of suspension parameters from their nominal values [22]. Robustness to modelling errors and parameter uncertainties must however be guaranteed in a real application and $H\infty$ thus becomes an attractive solution for railway active suspensions [3,9,19,23,24].

The principle of $H\infty$ control is illustrated in Figure 7, where the original open-loop system is expressed as G_0, and a control gain K_H is introduced with the objective of bounding the magnitude of the closed-loop transfer function T_{ed} from 'disturbance' d to 'error' e according to Eq. (18).

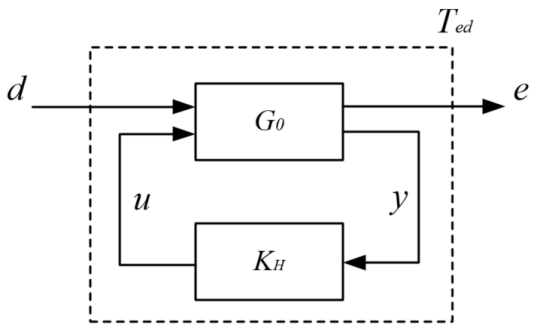

Figure 7 Control principle of H∞ control

$$\|T_{ed}(s)\|_\infty = \max_\omega \bar{\sigma}\left(T_{ed}(j\omega)\right) < \gamma \tag{18}$$

where, $\bar{\sigma}\left(T_{ed}(j\omega)\right)$ is the maximal singular value of T_{ed} in different frequency range; γ is a threshold value to be achieved for robustness.

The implementation of the $H\infty$ control for the mitigation of car-body vibration being the objective of this study is shown in Figure 8 for the case of active or semi-active secondary

suspensions. The schematic diagram of the $H\infty$ control is slightly different for the case of active or semi-active primary suspensions, due to the need to consider a double number of control forces.

The error vector *e* considers:

- the weighted accelerations of the car-body over the front bogie, at car-body centre and over the rear bogie (components e_1, e_2 and e_3 of the error vector);
- the weighted control efforts generated by the actuators or semi-active dampers (components e_4, e_5 for active/semi-active secondary suspensions and $e_4 \sim e_7$ for active/semi-active primary suspensions)

The disturbance vector includes the components of wheel vertical velocities $\dot{z}_w$ ($d_1 \sim d_4$) and wheel displacement z_w = ($d_5 \sim d_8$) and measuring noise for car-body accelerations ($d_9 \sim d_{11}$).

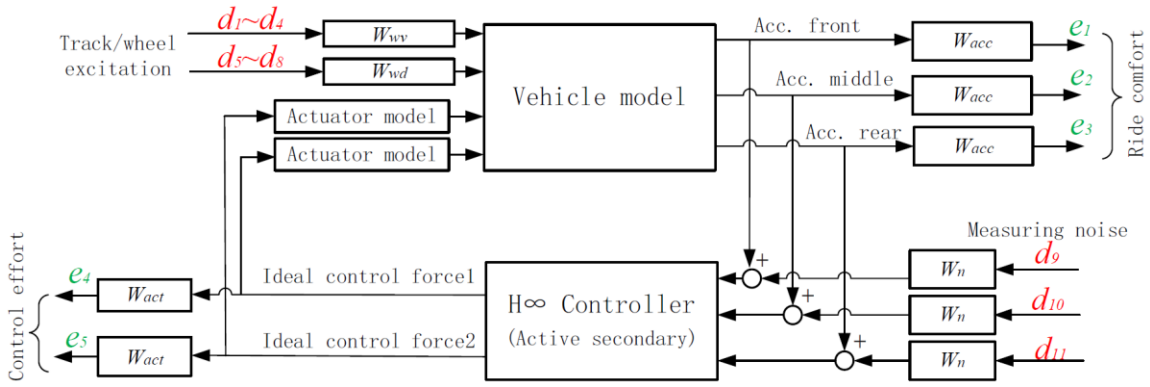

Figure 8 Arrangement of $H\infty$ control for active or semi-active secondary suspensions

In the implementation of $H\infty$ control proposed here, the actuator model is expressed as a first-order filter considering the response time of the actuator, see Eq. (8). The weighting functions $W_{acc}, W_{track}, W_{act}$ and W_n respectively weight frequencies of interest for the car-body acceleration, track irregularity, actuator force and measuring noise.

Frequency-dependent weight functions are introduced for each term in the error and disturbance vectors. The weight function W_{acc} for car-body acceleration is the ISO 2631 weighting curve for vertical vibration which is defined according to the human perception to mechanical vibrations at

different frequencies [25,26]. This weighting curve, shown in Figure 9 (a), implies that vibrations from 5Hz to 9Hz are the most relevant to vertical ride comfort. The weight function W_{act} for actuators' effort is chosen to have a sharp increase of the gain outside the actuator's passband, assumed from 0.1 to 10 Hz, see Eq. (19) and Figure 9(b). In this way, a penalty is introduced on controller commands outside the actuators' passband.

Regarding the transfer functions weighting the disturbance from track irregularities W_{wv} (for wheelset velocities $\dot{z}_w$) and W_{wd} (for wheelset displacements z_w), the approach proposed in [23] is followed. Data are collected for the vertical vibration of the wheelsets at the axle-box, considering the vehicle running at different speeds and PSD analyses are performed to synthesise the spectral components of the excitation. After many empirical tests, the weight functions W_{wv} and W_{wd} are defined, see Figure 9(c) and Eq. (20). The weight function for measuring noise W_n is defined in a similar way as W_{act}, see Figure 9(d) and Eq. (21), considering that noise normally appears in the low-frequency range below 0.1 Hz due to distortion in the accelerometer transducers and in the high-frequency above 100Hz due to electromagnetic disturbance in the measuring circuit [23]. All above-mentioned modules are assembled as shown in Figure 8 and finally the feedback gain matrix K_H is obtained solving the optimisation problem stated by Eq. (18) using MATLAB's function *hinfsyn*.

It is worth noting that a different choice of the frequency-dependent weighting functions would result in a different design of the H∞ controller. For instance, tuning of the weight functions can be used to shift the control effort towards a more effective mitigation of high-frequency structural vibrations at the expense of low-frequency vibration related to the rigid modes of the vehicle or vice-versa. The optimisation of the design of the H∞ controller is however beyond the scope of this work, whilst it is important to underline that the same weight functions were used for the four mechatronic suspension schemes considered (full-active / semi-active secondary and full-active / semi-active primary) to ensure an objective comparison.

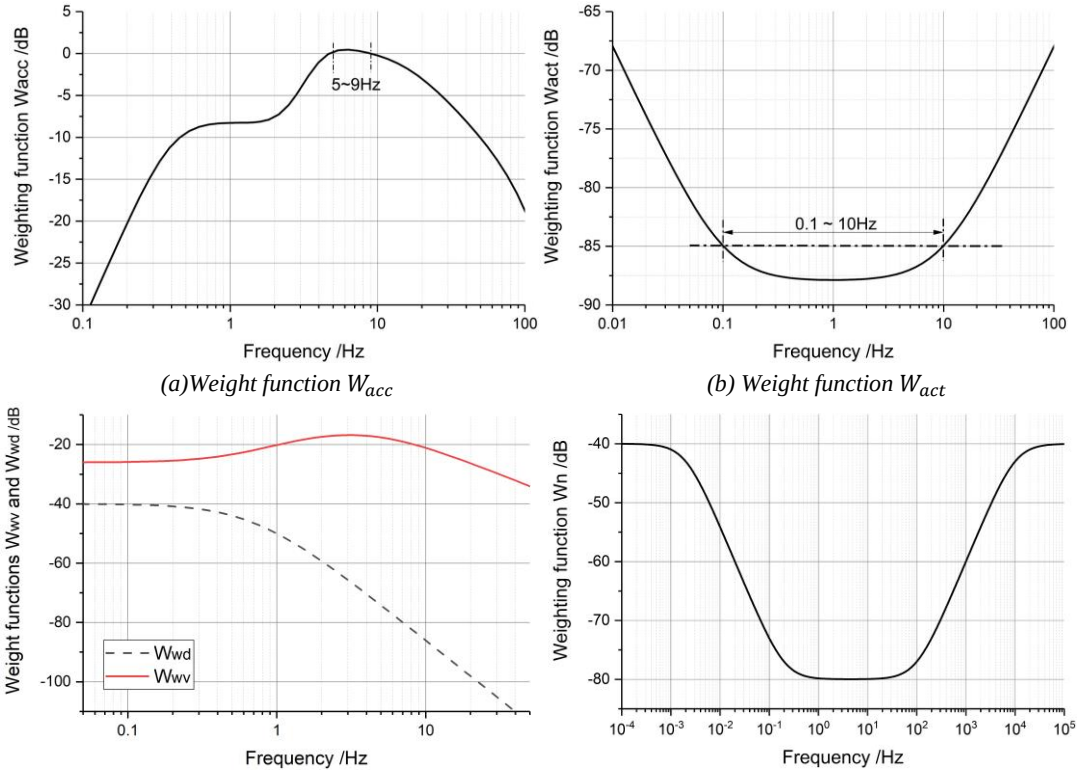

(a)Weight function W_{acc} *(b) Weight function W_{act}*

(c) Weight functions W_{wv} and W_{wd} *(d) Weight function W_n*

Figure 9 Curves for weight functions

$$W_{act} = 0.004 \cdot \frac{[(1+s/(0.1\cdot 2\pi)][(1+s/(15\cdot 2\pi)]}{[(1+s/(0.001\cdot 2\pi)][(1+s/(1500\cdot 2\pi)]} \tag{19}$$

$$\begin{cases} W_{wv} = \dfrac{0.05(1+s/(0.5\cdot 2\pi)}{[(1+s/(0.2\cdot 2\pi)][(1+s/(5\cdot 2\pi)]} \\ W_{wd} = \dfrac{0.01}{[(1+s/(0.5\cdot 2\pi)][(1+s/(1\cdot 2\pi)]} \end{cases} \tag{20}$$

$$W_n = 0.01 \cdot \frac{[(1+s/(0.2\cdot 2\pi)][(1+s/(100\cdot 2\pi)]}{[(1+s/(0.002\cdot 2\pi)][(1+s/(10000\cdot 2\pi)]} \tag{21}$$

4 Results of simplified model

In this section, the simplified vehicle model is used to investigate the benefits of using semi-active or full-active control in the primary and secondary suspensions. Depending on the case considered (full-active primary, semi-active primary, full active secondary, semi-active secondary) some of the passive dampers in the 9-DOF model shown in Figure 1 are replaced by actuators or

semi-active dampers. In all cases, a small amount of passive damping is maintained in the suspension where the active or semi-active component is introduced, to consider the minor damping effects due to the passive air spring in the secondary suspension and from primary springs. The residual passive damping considered is 10 kNs/m per bogie for the secondary suspension and 1 kNs/m per wheelset for the primary suspension.

All results presented in this section refer to the vehicle speed of 120 km/h and, unless differently specified, the response time of the actuators and semi-active dampers is set to 10 ms.

4.1 Results with LQG controller

For the case of active / semi-active secondary suspensions, the weight matrixes Q and R are defined as:

$$\begin{cases} Q = SF_{LQG} \cdot Diag(1 \times 10^4, 1 \times 10^4, 1 \times 10^4) \\ R = Diag(1 \times 10^{-4}, 1 \times 10^{-4}) \end{cases} (SF_{LQG} = 0.1, 0.167, 0.278 \dots, 10) \quad (22)$$

A scaling factor SF_{LQG} is applied to the Q matrix, allowing to consider different settings of the LQG controller in a range from a controller highly emphasising on low actuation forces (SF_{LQG} =0.1) to one highly emphasising on mitigating car-body accelerations (SF_{LQG} =10). Ten levels of the scaling factor are considered, growing from the lowest to the highest one in geometric progression with common ratio $r = 100^{\frac{1}{9}}$.

For the case of active / semi-active primary suspension, the Q matrix remains the same as defined in Eq. (22), while the R matrix becomes a four-by-four diagonal matrix with the same values of the non-zero terms as in Eq. (22). For semi-active secondary and primary suspensions, the damping force of controllable damper is derived from the actuator force through Eq. (9).

Figure 10(a) and (b) present the PSDs of car-body accelerations measured at car-body centre and over the front bogie, considering the four active/semi-active suspension options. The results are arranged in a four-quadrant order to facilitate the comparison of the four options.

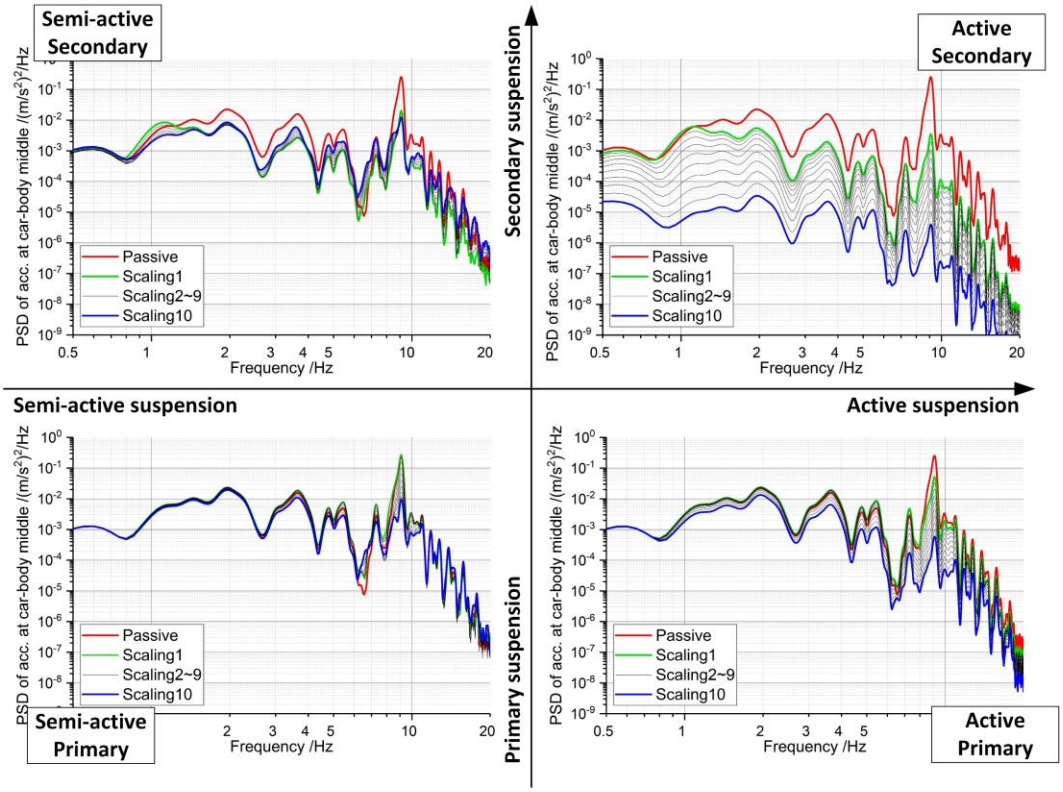

(a) PSDs of car-body vertical acceleration at car-body centre

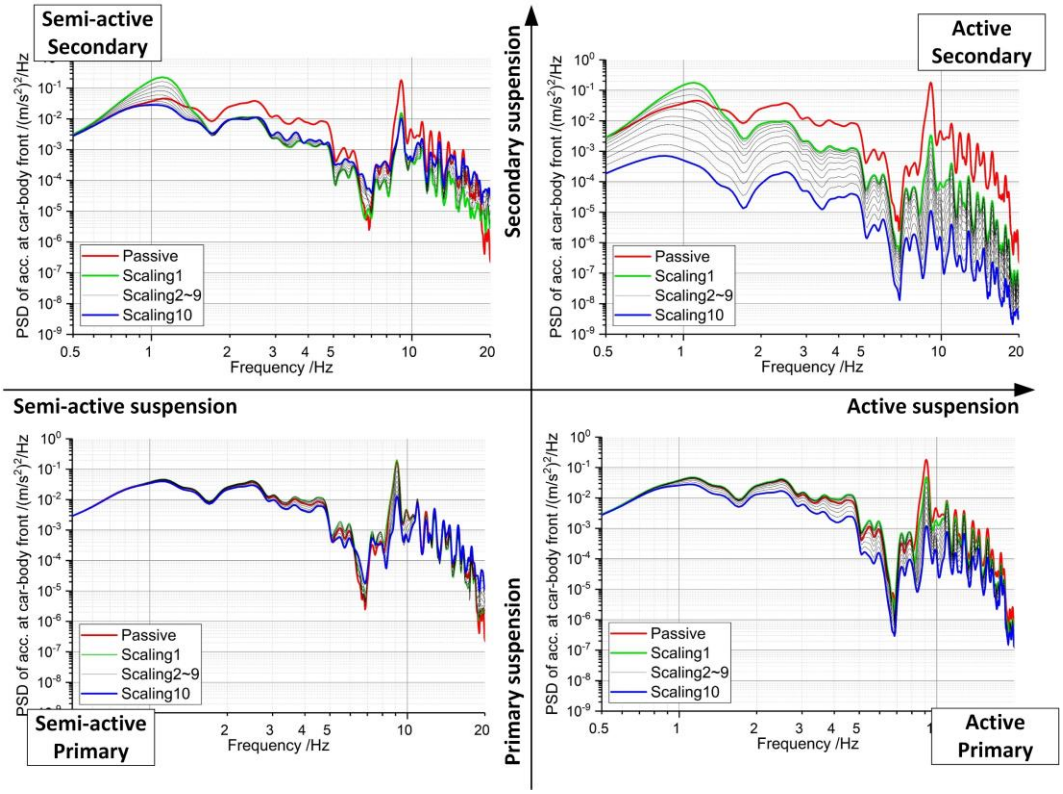

(b) PSDs of car-body vertical acceleration of the car-body over the front bogie

Figure 10 PSDs of acceleration under four suspension technologies

As shown in the right-top corner of Figure 10(a) and (b), full-active secondary suspension can effectively reduce the vibration at all frequencies even using a small value of the scaling factor SF_{LQG}. By contrast, the results obtained for the semi-active secondary suspension, in the left-top corner of the figures, is less effective than the full-active suspension, especially in respect of the rigid modes of the car-body but is still capable of attenuating the peak in the PSD related to the first bending mode of the car-body by more than a factor 10. The use of a relatively large scaling factor is required to avoid an increase of vibration in the frequency range around 1Hz which is related to the rigid modes of vibration of the car-body and is more clearly seen over the front bogie. The reason for the relatively bad performance of the semi-active secondary suspension in the frequency range around 1 Hz is that in this frequency range the rate of damper elongation/compression is low and therefore a much lower control force can be produced by the semi-active device compared to a full-active component.

Full-active primary suspension is presented in the right-bottom corner of Figure 10 and can reduce substantially car-body vibration in the frequency range from 5 Hz to 15 Hz but requires large values of the scaling factor SF_{LQG}. Car-body vibrations in the low-frequency range are also improved to some extent, at the expense of a large scaling factor, hence large actuator forces. Finally, semi-active primary suspension, shown in the left-bottom corner of the figures, provides a negligible improvement in the low-frequency range but is capable of attenuating very effectively vibration components related to car-body bending, reducing the peak of the PSD at 9 Hz by a factor above 10, provided a sufficiently large scaling factor is used. This remarkable performance is due to the fact that controlled primary suspensions can effectively mitigate bogie vibration in the high-frequency range thanks to the large rate of elongation/compression primary dampers undergo in the 5-15 Hz frequency range, thereby cutting drastically the amount of high-frequency vibration transmitted to the car-body.

In conclusion, as expected the active-secondary suspension provides the largest benefit in terms of reducing car-body vibration in the entire frequency range of interest. Active primary suspension

requires a larger control effort and can only improve the ride quality in the high-frequency range, so this is certainly a less attractive solution, even not considering implementation issues such as the need to fit active actuators in the narrow installation space of primary suspension and reliability issues due to the exposure of actuators to large vibrations. Semi-active primary suspension appears as an interesting option, as it provides significant attenuation of car-body vibration in the high-frequency range, but its advantage in the low-frequency range related to the rigid modes of the car-body is limited. From a practical point of view, it may be difficult to fit semi-active dampers having the required maximum damping in the secondary suspension, considering that many modern passenger vehicles are not including vertical dampers in the secondary suspension and instead are using orifice damping in the air spring to provide vertical secondary damping. Finally, semi-active primary suspension also provides a very effective reduction of vibration related to the car-body bending modes and at the same time benefits from a relatively simple implementation, as the passive primary dampers are replaced by controllable dampers that may have a similar size thereby easily fitting in the available installation space. Another advantage of semi-active primary suspension over mechatronic secondary suspensions is that the vibration of the bogie frame can also be reduced, reducing dynamic stresses in the frame itself and other components installed in the bogie, e.g. brake callipers.

4.2 Simulation results with $H\infty$ controller and comparison with LQG controller

Similar to the study of LQG control in sub-section 4.1, a scaling factor SF_{Hinf} is also introduced for $H\infty$ control, in the form of a weight applied to the W_{acc} function, i.e. using $SF_{Hinf} \cdot W_{acc}$ to express the importance in the control targets of car-body acceleration reduction. In this way, the $H\infty$ controller can be tuned to provide a more efficient reduction of car-body vibration or to require a lower control force. To get comparable results to LQG control, the ten levels for SF_{Hinf} range

from 0.3 to 3 according to a geometric progression with the same common factor used for SF_{LQG}, i.e. SF_{Hinf} = 0.3, 0.3875, 0.5004, …, 3.

The performance of the four active / semi-active options with $H\infty$ controller is compared in Figure 11 in terms of the PSDs of acceleration at car-body front, using the same representation as Figure 10 for the LQG controller. In the case of full-active secondary suspensions, the $H\infty$ controller is slightly less effective than the LQG controller with reducing the vibration of the car-body in the low-frequency range, but at the same time, $H\infty$ has slightly better performance than LQG in the high-frequency range. This difference comes from the fact that the weight function defined for the $H\infty$ favours a more focused effort of the control force in the frequency range 5-9Hz, which is according to ISO 2631 most relevant to vertical ride comfort.

The frequency-weighted effect of the $H\infty$ controller also affects the performance of the semi-active secondary suspension, see the left-top corner of Figure 11. Car-body vibrations in the 2~10 Hz frequency range are effectively reduced, but the PSDs at frequencies around 1Hz are higher compared to the passive vehicle, even for large values of the SF_{Hinf} scaling factor. One solution to this issue could be to use a different weight function W_{acc} in $H\infty$ controller so that more emphasis is placed by the controller on reducing vibrations in the low-frequency range, although this could somehow reduce the effectiveness of the controller at higher frequencies. Therefore, a proper design for semi-active secondary suspension needs to find a balance between controlling low-frequency and high-frequency vibrations of the car-body.

Finally, for full-active and semi-active primary suspensions the differences between the PSD curves obtained using the $H\infty$ and LQG controllers are minor.

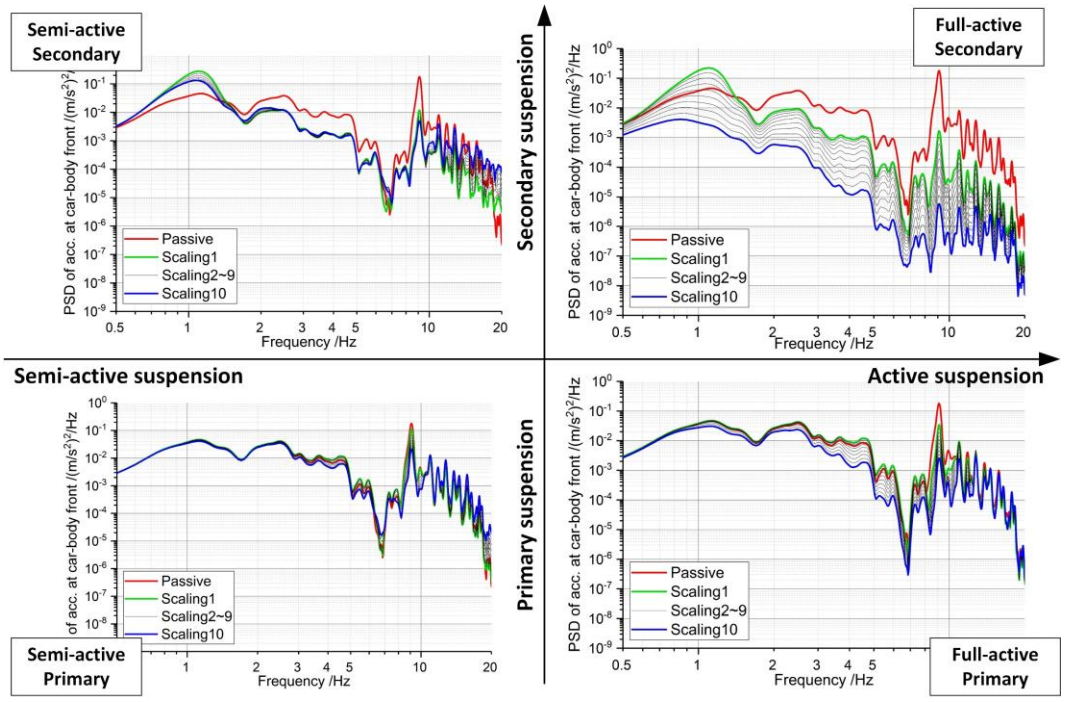

Figure 11 PSDs of car-body vertical acceleration over front bogie under four suspension technologies

To provide a more comprehensive comparison of the performance of the LQG and H∞ controllers, the RMS values of frequency-weighted acceleration according to ISO 2631 at vehicle speed 120 km/h are compared in Figure 12 for the four active/semi-active suspension options and for different values of the scaling factors SF_{LQG} / SF_{Hinf}. Figure 12(a) shows the results for the car-body point over the front bogie and Figure 12(b) for the centre of the car-body. The corresponding RMS values for the passive vehicle are shown in each plot by a horizontal dashed line with no markers.

As expected, the best performances are reached by full-active secondary suspensions, providing a substantial reduction of car-body vibration compared to the passive case even for low values of the scaling factor. Considering SF_{LQG} / SF_{Hinf} at level 1, the reduction of the RMS acceleration compared to the passive case is by a factor nearly 3 over the front bogie and by a factor 6 or more for the centre of the car-body. The better effect of active control in the car-body centre is due to the

fact that at this point the vibration of the car-body is more heavily affected by the resonance of the first bending mode. A further increase of the scaling factors provides a further reduction of the RMS, which, however, is probably not needed as the ride quality would be already very good for the relatively low levels of the scaling factor. Semi-active secondary suspensions also show a remarkable reduction of car-body vibration at both locations considered, but the improvement resulting from an increase of the scaling factors is limited. For the full-active primary suspension, the RMS acceleration at both locations decreases steadily with increasing levels of the scaling factors and becomes even lower than the semi-active secondary suspension when large scaling coefficients are applied. Finally, semi-active primary suspension, although providing the least reduction of the weighted RMS acceleration among the four options considered, can still reduce by a factor above 2 the vibrations at car-body centre compared to the passive vehicle, provided a sufficiently large scaling factor is used.

For the two full-active options, the performance obtained using the LQG and H∞ controllers are very similar, but for semi-active secondary suspensions the use of the LQG controller leads to a more effective attenuation of car-body vibration over the front bogie, compared to H∞, but at car-body centre the opposite situation is found, and a better performance is provided by the H∞ controller. This is due to the fact that $H\infty$ controller sets more emphasis of the control action on attenuating car-body vibrations in the 5~9Hz frequency range, and hence is capable of attenuating more effectively the vibration of the car-body at its centre, where the acceleration is more heavily affected by the first bending mode, but the attenuation over the bogies is less effective, as at these points the effect of rigid modes resonating at lower frequencies is more pronounced.

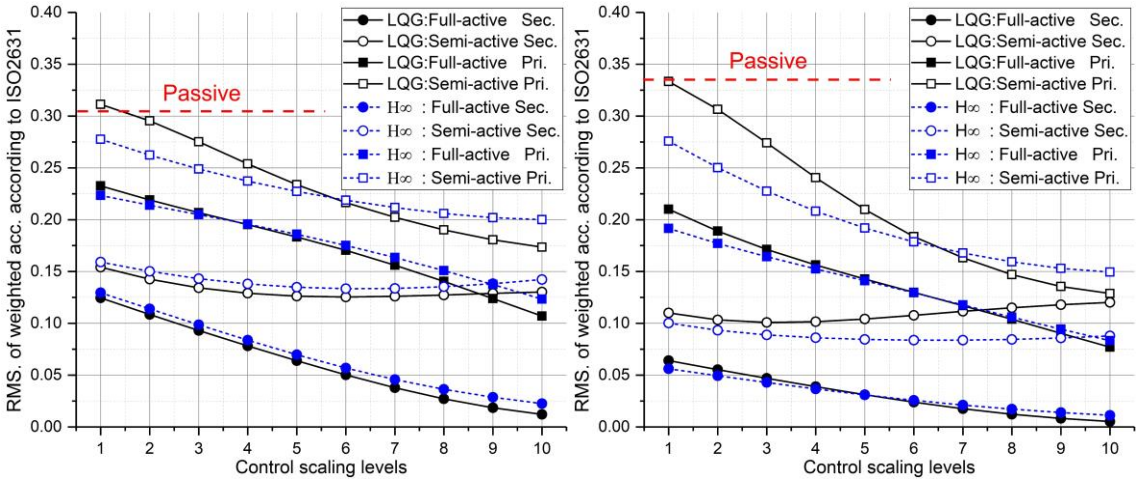

(a) Car-body front *(b) Car-body centre*

Figure 12 Comparison of RMS. of car-body vertical acceleration with LQG controller and H ∞ controller under four suspension technologies at (a)car-body front and (b)car-body centre at speed 120km/h

To focus on the suppression of car-body structural vibration related to the first bending mode, we extract the acceleration coming from the car-body first bending mode at 9 Hz, using a band-pass filter with frequency range specified from 8.5 to 9.5Hz, see Figure 13.

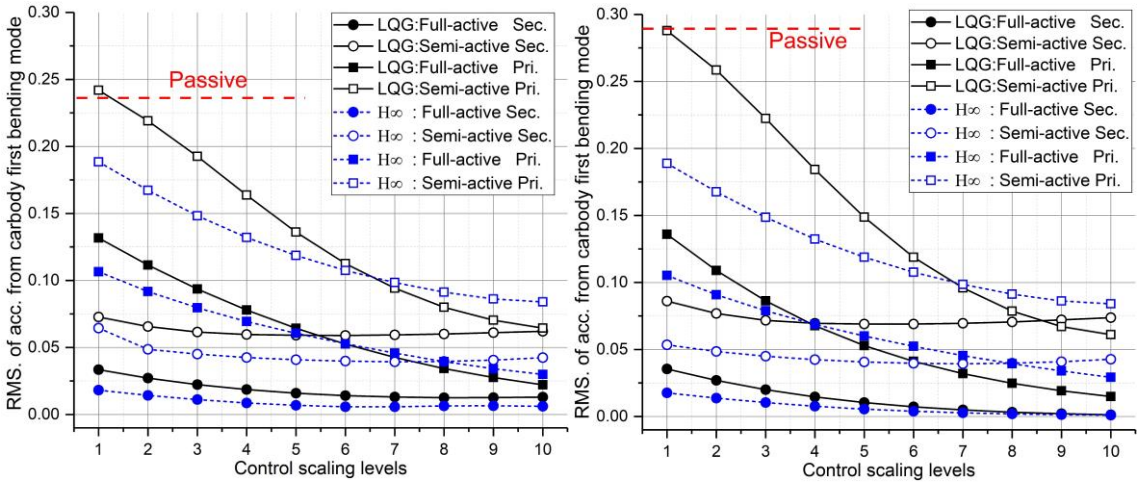

(a) Car-body front *(b) Car-body centre*

Figure 13 Comparison of RMS. of acceleration coming from car-body bending mode with LQG controller and H ∞ controller under four suspension technologies at (a)car-body front and (b)car-body centre at speed 120km/h

Semi-active primary suspension can reduce by 70-80% car-body first bending vibration if the largest scaling factor is chosen, either using LQG or $H\infty$ controller, which is a totally satisfactory performance. Other active/semi-active options still show a more effective mitigation of vibrations,

but the benefits become marginal and probably not sufficient to compensate for the ease of implementation allowed by semi-active primary suspensions.

Finally, Figure 14 compares the peak magnitude of the control force in full-active primary and secondary suspensions as a function of the scaling factor level, for the LQG and H∞ controllers. When large scaling factors are used, active primary suspensions require a peak force close to 15 kN, which may lead to a complex and expensive design of actuators. It should be recalled that the performance of full-active primary suspensions is highly depending on the intensity of the control action, see Figure 12, so this is another point advising against the use of full-active primary suspensions. The difference between the peak force implied by the use of LQG or H∞ controllers is limited for both active primary and active secondary and for all the scaling factors considered. The control force mentioned above is obtained based on the simplified two-dimensional model, where each bogie has one actuator for secondary suspension and two actuators for primary suspension. However, for the real vehicle, the number of actuators would be doubled, due to the symmetrical arrangement at left and right sides, which means that control force will be achieved by two actuators and each actuator capable of producing 8 kN force is enough to realize the highest control level in Figure 14.

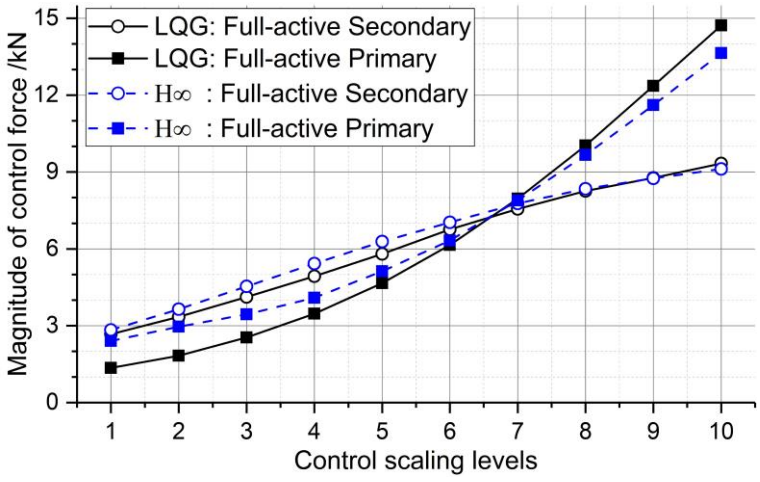

*Figure 14 Comparison of control force with LQG controller and **H** ∞ Controller*

It is also worth mentioning that in this paper a common sensor set-up considering the measure of car-body accelerations at three locations is used for all four mechatronic suspension schemes to enable an objective comparison among them. However, the real implementation of each mechatronic suspension scheme could be customized with different control targets, weight functions and sensor set-ups, according to the specific features of the technology adopted. One good example can be found in reference [6], where Sugahara used semi-active primary suspension to improve vertical ride comfort. Instead of using three car-body accelerations as the control target, the authors tried to separately control different vibration modes of the vehicle, including bounce and pitch motions of car-body and bogies and car-body first bending mode. This choice allows to put more emphasis on the mitigation of car-body bending modes rather than car-body rigid modes, focussing the use of semi-active primary suspension to a task that can be effectively performed by this suspension scheme.

4.3 Influence of response time of actuator/semi-active damper

In the simulations above, the response time of the actuator and the semi-active damper is set to 10ms using a first-order filter. This value might be achievable for fast semi-active dampers e.g. using a magneto-rheologic technology, but would be challenging for a full-active actuator, depending on the technologies considered [27]. In this section, the influence of the response time is studied. Using $H\infty$ control and a value SF_{Hinf} =1 of the scaling factor (approximately corresponding to scaling factor level 6 of SF_{Hinf} in the analysis presented in Section 4.2), simulations are repeated considering four different values of the response time increasing from 5ms to 30ms.

The results of this analysis are summarized in Table 2, where the weighted RMS of acceleration with the response time at 10ms is used as a reference to show the reduction and increase of RMS with faster and slower response times. Mechatronic suspension schemes mainly concerned with the

reduction of high-frequency vibration components are more sensitive to the time response of actuators or adjustable dampers. In particular, for semi-active primary suspensions the degradation of ride quality at car-body centre becomes very large (above 30%) if the response time is larger than 20 ms. Performance degradation is less critical for secondary suspensions, either full-active or semi-active, as vibration attenuation in the low-frequency range is affected to a lesser extent. The results obtained for the LQG controller are comparable and are not presented for the sake of brevity.

Table 2 Influence of response time of actuator/semi-active damper

Response time		5ms	10ms (RMS. of acc. m/s^2)	15ms	20ms	25ms	30ms
Full-active secondary	front	-0.06%	0% (0.060)	+0.59%	+1.67%	+3.20%	+5.08%
	centre	-0.32%	0% (0.027)	+1.33%	+3.59%	+6.68%	+10.49%
Semi-active secondary	front	-1.86%	0% (0.134)	+1.54%	+2.88%	+4.08%	+5.29%
	centre	-2.71%	0% (0.084)	+3.15%	+6.54%	+10.13%	+14.06%
Full-active Primary	front	-3.11%	0% (0.178)	+4.72%	+10.11%	+15.49%	+20.36%
	centre	0.04%	0% (0.133)	+2.68%	+7.59%	+14.07%	+21.39%
Semi-active Primary	front	-6.00%	0% (0.221)	+6.60%	+13.14%	+19.78%	+26.65%
	centre	-5.80%	0% (0.182)	+8.66%	+18.93%	+30.31%	+42.55%

5 Simulations based on full-scaled vehicle

The theory study based on the simplified 2-D model reveals the features of different technologies and shows significant improvement of ride quality using active or semi-active suspensions, but the working situation in the real case would be different as the 2-D model cannot accurately predict the real behaviours of the vehicle and excessive deviation between the real vehicle and the simplified model used in the design of the controller may lead to unsatisfactory performance. In this section, we explore the application of proposed control methods based on the simulation of a Flexible Multi-Body System (FMBS) vehicle model

Co-simulation between SIMPACK and SIMULINK is implemented, where FMBS model built in SIMPACK exports the three car-body accelerations and damper velocities (only for semi-active

control) to SIMULINK in which the controller receives the car-body acceleration and compute the control forces. These reference forces are fed to the simplified actuator/damper models, and the control forces are fed back to the FMBS model.

The $H\infty$ controller developed in Section 4.2 is adopted as it shows better robustness than the LQG controller, capable of dealing with model uncertainties and disturbance, which makes it a practical solution for real application. The configuration of the $H\infty$ controller is the same as is introduced in Section 4.2 for four suspension technologies. In the FMBS model, two actuators / controlled dampers are considered for each wheelset in mechatronic primary suspension, or for each bogie in the secondary suspension and the same reference force is defined for the two sides. The car-body roll motion has limited contribution to the vertical vibration, so the accelerometer sensors used by the H∞ controller are assumed to be installed along the centreline of the car-body. When (semi) active suspension technology is applied, the corresponding passive dampers are removed from the FMBS model but a small amount of passive damping is maintained in the suspension in the same way as done for the 9-DOF model. The response time of actuators and damper is set to 10ms.

Figure 15 shows the time histories of acceleration at car-body centre for the vehicle running at 120km/h and scaling factor SF_{Hinf}=1 in $H\infty$ control. The results show a significant reduction of car-body acceleration for all schemes, with full-active secondary suspension providing the best performance, as expected.

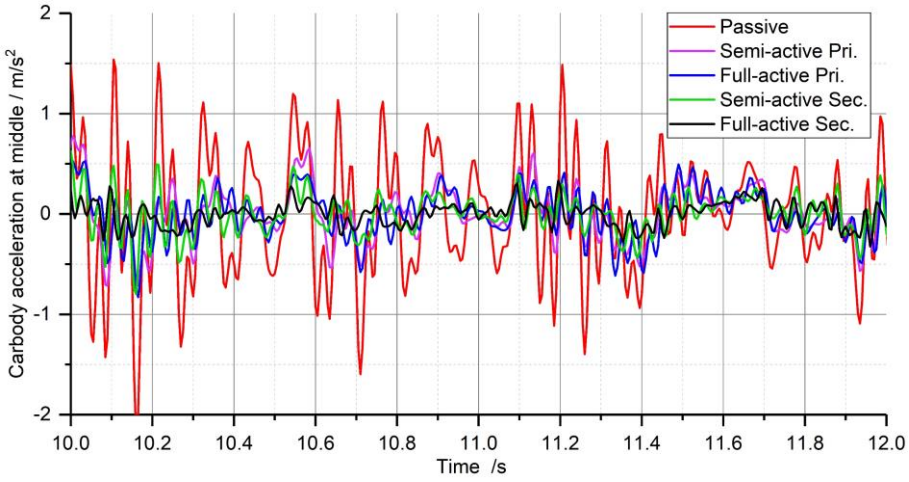

Figure 15 Time history of car-body vertical acceleration at centre position with different technologies

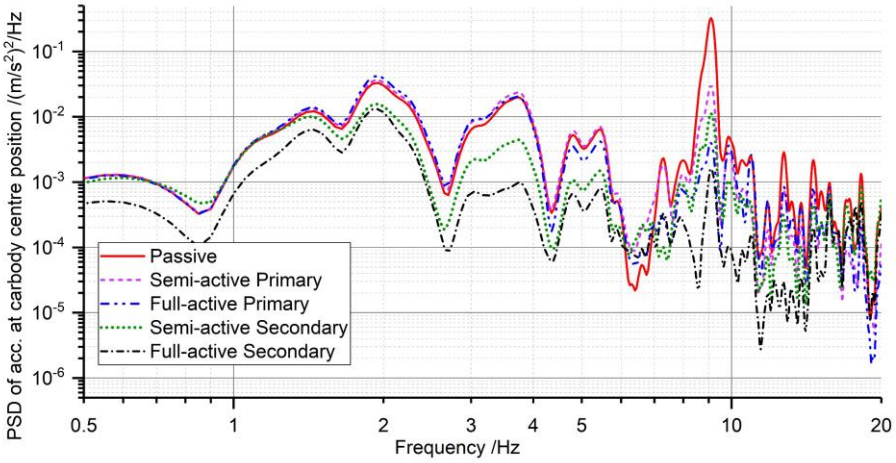

(a) PSD of car-body vertical acceleration at centre position

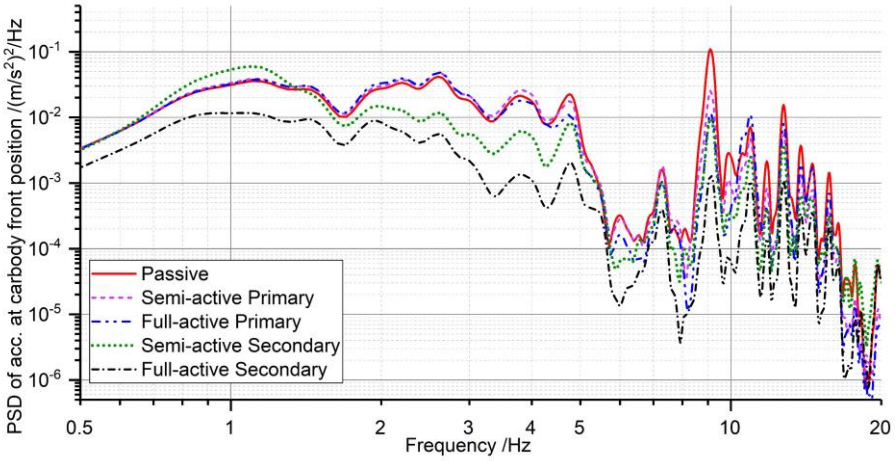

(b) PSD of car-body vertical acceleration at front position

Figure 16 Performance of the four (semi) active suspension technologies at speed 120km/h

The PSDs of car-body acceleration over the front bogie and at car-body centre are presented in Figure 16. These results confirm the conclusions obtained from the simplified 9-DOF model: the full-active secondary suspension effectively reduces car-body vibration in the entire frequency range of interest at both positions. The semi-active secondary suspension also mitigates car-body vibration in a wide frequency range but does not provide a benefit or even slightly increases the vibration at frequencies around 1 Hz. Furthermore, the reduction of the PSD peak at 9 Hz is less pronounced for semi-active secondary suspension compared to full-active secondary suspension. Semi-active primary suspension effectively mitigates vibration at 9Hz related to the first bending mode without negatively affecting ride comfort at lower frequencies. Full-active primary scheme shows further improvement at this resonance frequency and a broader frequency range of improved vibrations nearly from 7 to 10Hz.

The time histories of control force for active primary and active secondary suspension are presented in Figure 17, from which we can see that the maximum magnitude of control force for active secondary and primary suspension is 5 kN and 4 kN respectively, close to one half the magnitude of the force in Figure 14 for control level 6 (the nearest level to "SF_{Hinf}=1") and small enough to be realized by real actuators.

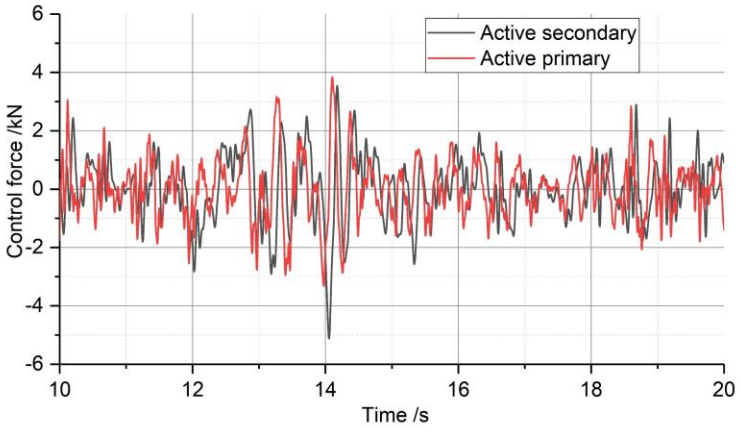

Figure 17 Time history of control force of active secondary and primary suspension

Figure 18 shows the trend with the speed of the RMS of car-body accelerations weighted by the filter in ISO 2631. For the passive vehicle, the results of the FMBS are in good agreement with those of the simplified 9-DOF model over the front bogie at 120km/h, the weighted RMS being 0.31 m/s^2 and 0.30 m/s^2 for the two models, but in the body centre the FMBS provides a larger value of the weighted RMS, 0.44 m/s^2 compared to 0.33 m/s^2 for the simplified model, due to the more detailed representation of car-body structural vibrations. The relatively simple semi-active primary suspension provides a reduction of the weighted RMS acceleration at car-body centre up to -44% at 120 km/h. This is less than the reduction predicted by the simplified model, see Figure 12(b), but is still very significant. The reduction of car-body vibration over the front bogie is less pronounced since the vibration of this point is less heavily affected by the bending modes. The benefit of full-active primary suspensions compared to semi-active primary suspensions is limited, whereas the results of the 9-DOF model show significant benefit of full-active primary vs. semi-active primary suspensions. This is due to the fact that the simplified model does not consider some details of the secondary suspensions (particularly the traction links) introducing a coupling between car-body bending and bogie pitch motion [28]. This topic is identified as the subject for a future extension of this work. Full-active and semi-active secondary suspensions are the best and second-best solutions, showing good improvement at all speed levels, providing approximately 70% and 50% reduction of frequency-weighted acceleration at both centre position and front position at 120km/h. However, there is no practical scope with going too far in the mitigation of car-body vibration, so probably a semi-active primary or secondary suspension can provide the required performance in regard of ride quality without the need to resort to the use of a more complex full-active secondary suspension.

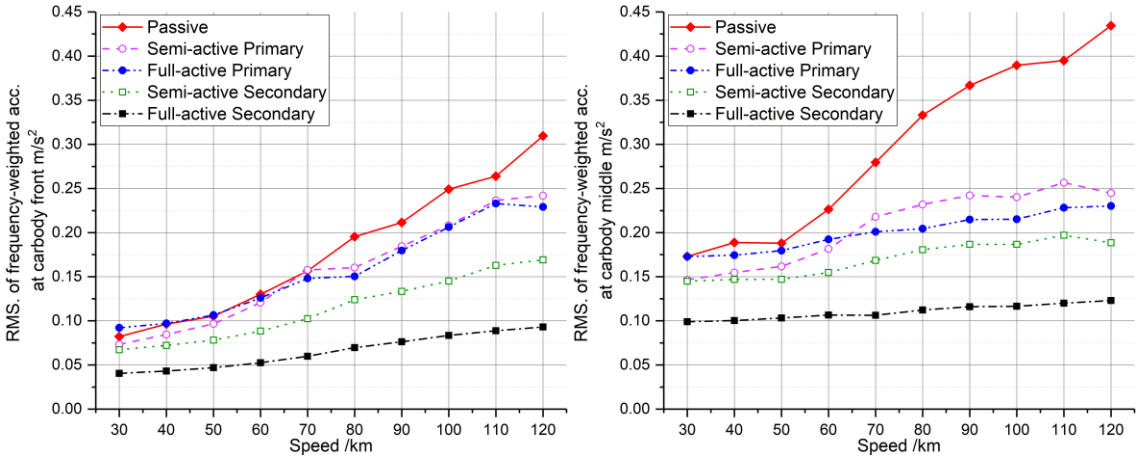

(a)Car-body front position *(b) car-body centre position*

Figure 18 the improvement of vertical ride comfort at different speed levels

6 Discussion and conclusions

In this paper, an objective comparison of the benefits of four configurations for mechatronic suspensions in railway vehicles: full-active primary, semi-active primary, full-active secondary and semi-active secondary suspensions, is investigated. The study is performed using two levels of detail in modelling the railway vehicle: a simplified 9-DOF model using Euler beam to represent the car-body bending modes and an FMBS model in which the flexible car-body is modelled based on the modal synthesis, with the modal parameters coming from a detailed finite element model of the car-body. The comparison of results from the two models shows a generally good agreement. Therefore, it is concluded that the simple and computationally effective 9-DOF model can be used to perform extensive sensitivity analyses and can also be used in the design of model-based control strategies for the mechatronic suspensions. However, the FMBS provides a better insight into the performance of the different mechatronic suspension options as far as the mitigation of car-body structural vibrations is concerned.

LQG and $H\infty$ controllers are considered in the study of the four mechatronic suspension schemes. The design of the controllers is performed in a consistent way for each scheme, to enable an objective comparative assessment of the four options.

Among the four configurations considered, full-active secondary suspensions show the best performance and provide excellent attenuation of low-frequency vibration related to the rigid modes of the car-body and, at the same time, of structural vibrations in a higher frequency range. Semi-active suspensions also provide good performance and could be preferred to full-active suspensions due to their lower cost and ease of implementation. Semi-active primary suspensions, although not suitable to mitigate low-frequency vibrations, provide a remarkable improvement of ride comfort in relation to the bending modes of the car-body. However, the good dynamic performance of the adjustable primary dampers is required, and the degradation of their performance is expected in case the response time is higher than 20 ms. Finally, full-active primary suspensions provide limited advantage compared to semi-active primary suspensions but involve a higher complexity and require large actuation forces. Apart from active primary suspension, all the other three schemes show high potential for future implementation. Full-active secondary suspension provides the best performance in terms of mitigating car body vibrations, but might not be the preferred solution depending on the extent to which a simpler arrangement of the suspension can be traded for reduced performance. Moreover, the safety and reliability of the actuation system are highly relevant to the selection and design of mechatronic suspensions [29].

An objective comparison of the suspension schemes from the perspective of ride comfort improvement needs a common set-up of controllers and sensors, as can been seen that minimizing car-body accelerations at three locations is used for all four mechatronic suspension schemes in the controller in this paper. However, it is worth recalling that the final implementation of a mechatronic suspension scheme should also consider other factors not addressed in this paper such as suspension deflection, weight functions and sensor set-up.

It should be noted that in this study the coupling of car-body bending with the pitch and longitudinal vibration of the bogies is neglected by the 9-DOF model due to the effect of the traction links and yaw dampers [28]. This effect is sufficiently weak for a low-speed vehicle like the one considered in this study, but for a high-speed vehicle equipped with yaw dampers, it may lead to

unacceptable deviation of the simplified model from the actual dynamic behaviour of the vehicle, which would, in turn, cause the failure of control strategies designed using the simplified model described in this paper. The nonlinear behaviour of the semi-active damper is not considered in this work. An extension of this study is envisaged to upgrade the 9-DOF model considering the coupling effects produced by the traction links and yaw dampers, and to consider a more realistic model of a magneto-rheologic damper to be used in the primary suspensions, moving forward to the application of the methods described in this paper to a real case.

Acknowledgement

The authors thank the company Blue Engineering and Design and Mr. Pierangelo Farina for sharing the finite element car-body model which is used in the FMBS model.

Disclosure Statement

No potential conflict of interest was reported by the authors.

ORCID

Bin Fu http://orcid.org/0000-0001-5024-4095

Stefano Bruni http://orcid.org/0000-0003-2177-5254

Appendix

Table A. Key parameters of full-scaled SIMPACK model

Parameters of the vehicle dynamics model	**Value [unit]**
Axle load (tare condition)	12[t]
Wheelbase	2500 [mm]
Base of bogie	19 [m]
Diameter of wheel (new)	860 [mm]
Wheel and rail profile	S1002/UIC60
Rail cant	1:40
Mass of car-body	34.25 [t]
Inertia moments of car-body Ixx/Iyy/Izz	8.29e4/2.31e7/2.29e7[kgm^2]
Mass of frame	3 [t]
Inertia moments of frame Ixx/Iyy/Izz	1480/2200/2800[kgm^2]
Mass of wheel-set	1.8 [t]
Stiffness of primary coil spring in x/y/z direction	1.8/1.8/1.3 [MN/m]
Damping of primary damper (passive)	15 [kN/m/s]
Stiffness of air-spring in x/y/z directions	0.2/0.2/0.35 [MN/m]
Damping of air-spring in z directions	10 [kN/m/s]
Longitudinal stiffness of traction link bushing component	10 [MN/m]
Longitudinal stiffness of traction rod bushing component	8 [MN/m]
Secondary vertical damper (passive)	40 [kN/m/s]
Secondary lateral damper (passive)	60 [kN/m/s]
Equivalent stiffness of anti-roll bar	1.5 [MN/rad]

References

[1] S. Bruni, R. Goodall, T.X. Mei, H. Tsunashima, Control and monitoring for railway vehicle dynamics, User Model. User-Adapt. Interact. 45 (2007) 743–779. https://doi.org/10.1080/00423110701426690.

[2] R. Goodall, Active railway suspensions: Implementation status and technological trends, Veh. Syst. Dyn. 28 (1997) 87–117. https://doi.org/10.1080/00423119708969351.

[3] B. Fu, R.L. Giossi, R. Persson, S. Stichel, S. Bruni, R. Goodall, Active suspension in railway vehicles: a literature survey, Railw. Eng. Sci. (2020). https://doi.org/10.1007/s40534-020-00207-w.

[4] G. Diana, F. Cheli, A. Collina, R. Corradi, S. Melzi, The Development of a Numerical Model for Railway Vehicles Comfort Assessment Through Comparison With Experimental Measurements, Veh. Syst. Dyn. 38 (2002) 165–183. https://doi.org/10.1076/vesd.38.3.165.8287.

[5] J. Zhou, R. Goodall, L. Ren, H. Zhang, Influences of car body vertical flexibility on ride quality of passenger railway vehicles, Proc. Inst. Mech. Eng. Part F J. Rail Rapid Transit. 223 (2009) 461–471. https://doi.org/10.1243/09544097JRRT272.

[6] Y. Sugahara, A. Kazato, R. Koganei, M. Sampei, S. Nakaura, Suppression of vertical bending and rigid-body-mode vibration in railway vehicle car body by primary and secondary suspension control: Results of simulations and running tests using Shinkansen vehicle, Proc. Inst. Mech. Eng. Part F J. Rail Rapid Transit. 223 (2009) 517–531. https://doi.org/10.1243/09544097JRRT265.

[7] R. Goodall, G. Freudenthaler, R. Dixon, Hydraulic actuation technology for full- and semi-active railway suspensions, Veh. Syst. Dyn. 52 (2014) 1642–1657. https://doi.org/10.1080/00423114.2014.953181.
[8] A. Qazizadeh, R. Persson, S. Stichel, On-track tests of active vertical suspension on a passenger train, Veh. Syst. Dyn. 53 (2015) 798–811. https://doi.org/10.1080/00423114.2015.1015429.
[9] T. Kamada, K. Hiraizumi, M. Nagai, Active vibration suppression of lightweight railway vehicle body by combined use of piezoelectric actuators and linear actuators, Veh. Syst. Dyn. 48 (2010) 73–87. https://doi.org/10.1080/00423111003668237.
[10] G. Schandl, P. Lugner, C. Benatzky, M. Kozek, A. Stribersky, Comfort enhancement by an active vibration reduction system for a flexible railway car body, Veh. Syst. Dyn. 45 (2007) 835–847. https://doi.org/10.1080/00423110601145952.
[11] E. Foo, R.M. Goodall, Active suspension control of flexible-bodied railway vehicles using electro-hydraulic and electro-magnetic actuators, Control Eng. Pract. 8 (2000) 507–518. https://doi.org/10.1016/S0967-0661(99)00188-4.
[12] C. Huang, J. Zeng, G. Luo, H. Shi, Numerical and experimental studies on the car body flexible vibration reduction due to the effect of car body-mounted equipment, Proc. Inst. Mech. Eng. Part F J. Rail Rapid Transit. 232 (2018) 103–120. https://doi.org/10.1177/0954409716657372.
[13] Q. Wang, J. Zeng, Y. Wu, B. Zhu, Study on semi-active suspension applied on carbody underneath suspended system of high-speed railway vehicle, JVC/Journal Vib. Control. 26 (2020) 671–679. https://doi.org/10.1177/1077546319889863.
[14] Y. Sugahara, A. Kazato, T. Takigami, R. Koganei, Suppression of vertical vibration in railway vehicles by controlling the damping force of primary and secondary suspensions, Q. Rep. RTRI (Railw. Tech. Res. Institute). 49 (2008) 7–15. https://doi.org/10.2219/rtriqr.49.7.
[15] Y. Sugahara, T. Kojima, Suppression of vertical vibration in railway vehicle carbodies through control of damping force in primary suspension: Presentation of results from running tests with meter-gauge car on a secondary line, WIT Trans. Built Environ. 181 (2018) 329–337. https://doi.org/10.2495/CR180301.
[16] S.S. Rao, Vibration of Continuous Systems, Second Edi, Wiley, 2019. https://doi.org/10.1017/CBO9781107415324.004.
[17] BS ISO 2631-4:2001+A1:2010. Mechanical vibration and shock-Evaluation of human exposure to whole-body vibration, (n.d.).
[18] Y. Sugahara, A. Kazato, R. Koganei, M. Sampei, S. Nakaura, Suppression of vertical bending and rigid-body-mode vibration in railway vehicle car body by primary and secondary suspension control : results of simulations and running tests using Shinkansen vehicle, (2009) 2–8. https://doi.org/10.1243/09544097JRRT265.
[19] L.-H. Zong, X.-L. Gong, S.-H. Xuan, C.-Y. Guo, Semi-active H∞ control of high-speed railway vehicle suspension with magnetorheological dampers, Veh. Syst. Dyn. 51 (2013) 600–626. https://doi.org/10.1080/00423114.2012.758858.
[20] F. YU, D.A. CROLLA, An Optimal Self-Tuning Controller for an Active Suspension, Veh. Syst. Dyn. 29 (1998) 51–65. https://doi.org/10.1080/00423119808969366.
[21] D.A. Wilson, R.S. Sharp, S.A. Hassan, The Application of Linear Optimal Control Theory to the Design of Active Automotive Suspensions, Veh. Syst. Dyn. 15 (1986) 105–118. https://doi.org/10.1080/00423118608968846.
[22] J.C. Doyle, Guaranteed Margins for LQG Regulators, IEEE Trans. Automat. Contr. 23 (1978) 756–757. https://doi.org/10.1109/TAC.1978.1101812.
[23] A. Orvnäs, S. Stichel, R. Persson, Active lateral secondary suspension with H ∞ control to improve ride comfort: simulations on a full-scale model, Veh. Syst. Dyn. 49 (2011) 1409–1422. https://doi.org/10.1080/00423114.2010.527011.

[24] A. Qazizadeh, S. Stichel, H.R. Feyzmahdavian, Wheelset curving guidance using H∞ control, Veh. Syst. Dyn. 56 (2018) 461–484. https://doi.org/10.1080/00423114.2017.1391396.
[25] K. Knothe, S. Stichel, Rail vehicle dynamics, 2016. https://doi.org/10.1007/978-3-319-45376-7.
[26] ISO, Mechanical vibration and shock-Evaluation of human exposure to whole body vibration- Part 4:Guidelines for the evaluation of the effects of vibration and rotational motion on passenger and crew comfort in fixed guideway transport systems. ISO 2631-4. Inte, 2001.
[27] Research report of project RUN2RAIL,Deliverable 3.1 – State of the art actuator technology,http://www.run2rail.eu/Page.aspx?CAT=DELIVERABLES&IdPage=06c1be36-4a7a-42e8-9bed-bfe71c3134be, 2018.
[28] T. Tomioka, T. Takigami, Reduction of bending vibration in railway vehicle carbodies using carbody–bogie dynamic interaction, Veh. Syst. Dyn. 48 (2010) 467–486. https://doi.org/10.1080/00423114.2010.490589.
[29] B. Fu, S. Bruni, Fault-tolerant design and evaluation for a railway bogie active steering system, Veh. Syst. Dyn. (2020) 1–25. https://doi.org/10.1080/00423114.2020.1838563.